Plant, Cell and Environment (1997) **20,** 867–880

Qualitative effects of patchy stomatal conductance distribution features on gas-exchange calculations

T. N. BUCKLEY[1], G. D. FARQUHAR[2] & K. A. MOTT[1]

[1]*Department of Biology, Utah State University, Logan, Utah 84322-5305, USA and* [2]*Environmental Biology Group, Research School of Biological Sciences, Australian National University, GPO Box 475, Canberra City, ACT 2601, Australia*

ABSTRACT

The qualitative influence of patchy stomatal conductance distributions on the values of photosynthesis (A) and intercellular CO_2 concentration (c_i) as determined by gas-exchange measurements were investigated using computer modelling. Gas-exchange measurements were simulated for different conductance distributions by modelling photosynthesis explicitly for each patch, summing these rates, and inferring c_i from a diffusion equation. Qualitative relationships are presented between conductance distribution features and the difference between assimilation rates measured for patchy and homogeneous leaves at the same c_i (A_p and A_h, respectively). These data show that, although most conductance distributions have little effect on the value of A measured for a given c_i, some distribution features (which we have termed 'bimodality', 'position', 'skewness' and 'range') play a key role in controlling the magnitude of these effects. Distributions that are more nearly bimodal, span regions of lower conductance, are right-skewed, or have broader conductance ranges are associated with larger effects on the $A(c_i)$ relationship. To clarify our mathematical analysis and illustrate some of the trends it predicts, we present conductance distributions and gas-exchange data from leaves of *Malus dolgo* var. Spring Snow that were treated with ABA. The results are discussed in the light of recent controversy over the effect of patchy stomatal conductance on gas-exchange data.

Key-words: crabapple; A versus c_i curve; CO_2, computer modelling; gas exchange; patchy; photosynthesis; stomata.

INTRODUCTION

Patchy stomatal behaviour can influence the relationship between the CO_2 assimilation rate (A) and intercellular CO_2 mole fraction (c_i) measured by gas-exchange methods. The assimilation rate measured under patchy conditions (A_p) for a given value of c_i is generally lower than the value measured under homogeneous stomatal behaviour (A_h) for the same c_i (Terashima *et al.* 1988; Cheeseman 1991; Terashima 1992). When and if this decrease becomes significant, it creates ambiguity in studies of photosynthesis: to what extent does a reduction in A for a given value of c_i reflect changes in the pattern of stomatal opening, rather than a reduction in the capacity for photosynthesis at the chloroplast level (Terashima 1992)? Stomatal patchiness therefore represents a possible source of error in studies of photosynthesis, because it can cause decreases in the observed relationship between A and c_i in addition to any real changes which may occur in the photosynthetic capacity of the leaf (Terashima *et al.* 1988; Farquhar 1989; Raschke *et al.* 1990; van Kraalingen 1990; Terashima 1992).

The potential magnitude and significance of artefacts caused by patchiness have been the subject of much research and debate in recent years (e.g. Terashima *et al.* 1988; Robinson, Grant & Loveys 1988; Raschke *et al.* 1990; Cheeseman 1991; Gunasekera & Berkowitz 1992; Terashima 1992; Beyschlag, Pfanz & Ryel 1992; Mott, Cardon & Berry 1993; Hirasawa *et al.* 1995; Mott 1995). Cheeseman (1991) presented a theoretical analysis based on computer modelling, and concluded that stomatal heterogeneity 'has little effect on the estimation of c_i.' However, his work started from the assumption that 'the distribution of conductances in any leaf area is "bell-shaped" ' (Cheeseman 1991), and therefore only addressed cases in which stomatal conductance (g) exhibited a statistically 'normal' distribution. Empirical observations suggest that other types of distributions often underlie stomatal patchiness (van Gardingen, Jeffree & Grace 1989; Raschke *et al.* 1990; Beyschlag *et al.* 1992; Mott *et al.* 1993; Mott 1995).

Furthermore, while some data show that patchiness can occur without significantly altering the observed relationship between A and c_i (Mott 1995), other data show that patchiness is often observed in association with large differences between A_h and A_p for a given c_i (e.g. Terashima *et al.* 1988; Raschke *et al.* 1990; Beyschlag *et al.* 1992; Epron & Dreyer 1993; Mott 1995). These observations together with Cheeseman's work (1991) suggest that only certain types of patchy conductance distributions can have large effects on the A versus c_i relationship measured by gas exchange. However, more information is needed to determine what types of distributions have large effects.

In this study, we present a mathematical analysis illustrating the qualitative effects of various patchy conductance

Correspondence: Keith A. Mott, Department of Biology, Utah State University, Logan, UT 84322-5305, USA.

distributions on the values of A and c_i that would be calculated from gas-exchange data. The goal of this study was to identify conductance distributions that have large effects on measured values of A and c_i; these effects in no way preclude changes in A and c_i caused by changes in mesophyll functioning, which may occur separately from, or concurrently with, patchy stomatal closure. In our analysis, we constructed a model of a leaf with heterogeneous stomatal conductance and calculated CO_2 assimilation explicitly for each patch. To make our analysis as widely applicable as possible, and in view of the general dearth of data on conductance distributions in real leaves, we used several different types of conductance distributions spanning wide ranges of conductance. From the analysis it was possible to identify several qualitative features of conductance distributions that have large effects on the difference between A_h and A_p for a given c_i.

To help clarify our mathematical analysis and relate it to real leaves, we compared some of the model's qualitative predictions with trends observed between distribution features and differences between A_h and A_p in two patchy leaves. Finally, we provide an example of how one might investigate the usefulness of the model's *quantitative* predictions by comparing the *absolute* differences predicted by the model with the differences observed by gas exchange for the patchy leaves.

MATERIALS AND METHODS

Patchy conductance model

Variable numbers of 'patches' (regions of the leaf with uniform conductance) were defined in the model, each with its own value for g. The number of patches that shared a given value of g was determined by a different conductance distribution in each model run. A very broad set of distribution features was used in these model runs, because no clear generalizations can be drawn from the existing data (e.g. van Gardingen *et al.* 1989; Daley *et al.* 1989; Beyschlag *et al.* 1992; Mott *et al.* 1993; Mott 1995) concerning the types of distributions that occur in real leaves. Our analysis will therefore address some distributions representing extremes of certain qualitative features; we do not wish to imply that such extremes actually occur in real leaves. Their inclusion is required for complete elucidation of the qualitative trends between distribution features and effects on the relationship between A and c_i.

For each conductance distribution we determined two values of A: one value for the patchy distribution (A_p), and one value for a homogeneous distribution that would yield the same measured c_i as the patchy distribution using gas-exchange techniques (A_h). This procedure is equivalent to comparing the $A(c_i)$ curves for the two distributions at one c_i value. However, when making gas-exchange measurements under patchy stomatal conditions, it is extremely difficult to obtain a complete A versus c_i curve without altering the prevailing conductance distribution. Therefore, a single point for A and c_i is usually compared to a full A versus c_i relationship determined under non-patchy conditions. In our analysis we have mimicked this procedure by comparing values of A for non-patchy and patchy conductance distributions at a single value of c_i. This is described graphically in Fig. 1, which will be referred to repeatedly below.

To calculate the values for A and c_i that would be measured by gas exchange for the patchy leaf (A_p and c_{ip}, respectively), and for a homogeneous leaf (A_h and c_{ip}) with the same c_i, the following procedure was carried out for each distribution:

(1) The assimilation rate for each patch was determined from the photosynthesis model described in Appendix A, using a value for stomatal conductance given by the distribution under study, and using parameters given in Table 1.
(2) The whole-leaf assimilation rate that would be measured by gas exchange (A_p) was calculated by averaging the assimilation rates for all patches (note that this implicitly defines all patches to be of equal area). Having calculated A_p, we can imagine drawing the lower of the two horizontal dotted lines in Fig. 1 – the one going through 'A_p'.
(3) The intercellular CO_2 mole fraction for the patchy leaf (c_{ip}) was estimated by the same mathematical procedure used in gas-exchange calculations: solving a CO_2 diffusion equation for c_i, using the *whole-leaf* values for assimilation and conductance. This is shown in Eqn 1:

$$c_{ip} = c_a - \frac{A_{leaf}}{g_{leaf}} = c_a - \frac{A_p}{g_{average}} \cdot \qquad (1)$$

Since all patches were of equal area, the whole-leaf conductance (g_{leaf} and $g_{average}$ in Eqn 1) was simply calculated by

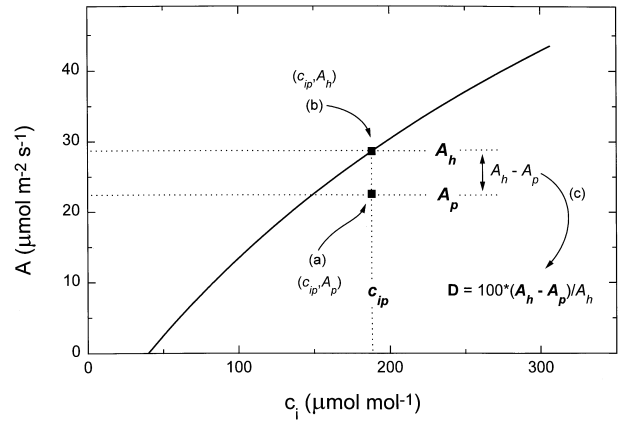

Figure 1. Diagrammatic representation of the relationship between A_h, A_p and c_{ip} as discussed in the text. The solid line is the 'homogeneous' $A(c_i)$ curve obtained from the biochemical model (Eqns A1 and A2, Appendix A). The lower square symbol, indicated by an arrow from '(a)', represents the point (c_{ip}, A_p), where c_{ip} is the estimate of c_i given by gas-exchange calculations from a patchy leaf, and A_p is the photosynthetic rate for the patchy leaf. The upper square symbol, indicated by an arrow from '(b)', is the point (c_{ip}, A_h); A_h is the photosynthesis rate one would expect to measure in association with c_{ip}. The double-ended arrow indicates the difference between A_h and A_p, and the curved arrow '(c)' points from this difference to the equation for D, showing the graphical meaning of D.

Parameter	Value	Meaning
$V_{c,max}$	125 μmol m^{-2} s^{-1}	Maximum carboxylation velocity[1]
K_c	318 μmol mol^{-1}	Michaelis constant for CO_2[2]
K_o	$4{\cdot}71\times10^5$ μmol mol^{-1}	Michaelis constant for O_2[2]
O	$2{\cdot}10\times10^5$ μmol mol^{-1}	Partial pressure of O_2
J	300 μmol(e$^-$) m^{-2} s^{-1}	Light-saturated potential rate of electron transport
R_d	0 μmol m^{-2} s^{-1}	Dark respiration rate
c_a	350 μmol mol^{-1}	Partial pressure of CO_2
Γ_*	40 μmol mol^{-1}	CO_2 compensation point without dark respiration

Table 1. List of parameters used for photosynthesis model. Sources: [1]Farquhar *et al*. (1980); [2]Woodrow & Berry (1988)

averaging the conductance values for all patches. This gas-exchange estimate of c_i defines the vertical dotted line in Fig. 1, and identifies the point (c_{ip}, A_p).

(4) The whole-leaf assimilation rate for the homogeneous case (A_h) was determined from the biochemical model, using the c_i value calculated for the patchy case (c_{ip}). To understand why A_h was calculated in this way, recall that we were comparing patchy and homogeneous distributions *at the same value of* c_i. In other words, A_h is the assimilation rate that one would expect to observe in association with c_{ip} if the stomata were instead behaving uniformly. In Fig. 1, this is the value of A on the 'homogeneous' $A(c_i)$ curve that corresponds to c_{ip}. Therefore, A_h is simply $A(c_{ip})$ from the biochemical model.

The difference between A_h and A_p was then calculated and expressed as a 'percentage deviation' or 'percentage difference' and termed 'D'. [Note that this value is the complement of the term '%A' in Mott (1995), in that the two numbers add to unity: D + %A = 100%.] This entire procedure was performed for many types of conductance distributions, and trends between D and various distribution features are presented and discussed. (A more rigorous description of the modelling procedures, including the equations, can be found in Appendix A.)

To help clarify this mathematical analysis and relate it to real leaves, we applied similar procedures (described in detail in Appendix B) to two patchy conductance distributions obtained from chlorophyll fluorescence images of leaves of crabapple (*Malus dolgo* var. Spring Snow). The frequency histograms for conductance and the value of D (both corresponding to a single moment in time) were calculated for each image and were used to test the model's qualitative predictions concerning D for various types of conductance distributions. Finally, the absolute differences predicted by the model were compared with those observed by gas exchange, to give an example of the type of analysis that would be necessary to test the model's quantitative predictions and determine whether distributions causing large differences between A_h and A_p actually occur in leaves.

Gas exchange

Leaves of crabapple (Malus dolgo var. Spring Snow) were enclosed in a gas-exchange chamber, and data were collected using a standard single-pass gas-exchange system as described previously (Mott 1995). Conditions were as follows: leaf temperature = 25 ± 0·1 °C; Δw (the water vapour mole fraction gradient between leaf and atmosphere) = 14·1 ± 0·4 mmol mol^{-1}; photon flux density = 1000 μmol m^{-2} s^{-1}; ambient CO_2 mole fraction (c_a) = 290 μmol mol^{-1} (14 May 1992), 320 μmol mol^{-1} (25 June 1992); ambient O_2 mole fraction = 2% (20 mmol mol^{-1}). For each leaf, a relationship was obtained between steady-state photosynthetic CO_2 assimilation rate (A) and intercellular CO_2 partial pressure (c_i) under conditions of homogeneous stomatal conductance [c_a was varied between 50 μmol mol^{-1} and the experimental value (290 or 320 μmol mol^{-1}) to obtain these A versus c_i curves]. Patchy stomatal closure was induced by the application of a pulse of abscisic acid through the transpiration stream (14 May 1992: 10 mmol m^{-3} ABA for 45 s, total dose = 20 nmol m^{-2} ABA; 25 June 1992: 10 mmol m^{-3} ABA for 62 s, total dose = 15 nmol m^{-2} ABA). Images of chlorophyll fluorescence were obtained and converted to images of 'q_n' as described previously (Mott 1995). For each day, a single image corresponding to the maximum difference between A_h and A_p at a given c_i was chosen for detailed analysis. The procedures used to calculate stomatal conductance distributions from these images and to predict differences between A_h and A_p are described in detail in Appendix B.

Distribution features

Several important features of stomatal conductance distributions emerged from preliminary efforts. These included the range, position, bimodality and skewness of distributions (as explained below). To examine these features, two basic types of discrete conductance distributions were constructed: 'even' and 'triangular.' It is critical to note that these distributions were not intended to represent conductance distributions that occur in real leaves. Rather, they were mathematical abstractions whose features could be easily manipulated to determine the *qualitative* relationships between such isolated abstract features and changes in the relationship between A and c_i.

The first class of distributions examined were 'even' distributions, which have equal numbers of patches at each of several values of conductance. These appear 'flat,' as in Figs 2a and 2b, and were varied in form by adjusting three key features. First, the *range* of conductance spanned by

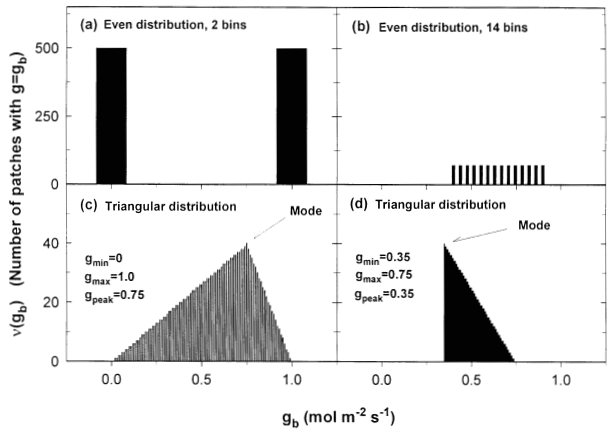

Figure 2. Examples of 'even' and 'triangular' conductance distributions used in the model. (a) Even distribution with 2 conductance bins (b = 2, so there are 1000/b = 500 patches in each bin), and a range of 1·0 mol m^{-2} s^{-1} defined by g_{min} = 0·0 and g_{max} = 1·0. (b) Even distribution with 14 bins and 71 patches in each bin (1000 patches/14 bins = 71·43≈71 patches/bin), and a range of 0·50 mol m^{-2} s^{-1} defined by g_{min} = 0·40 and g_{max} = 0·90. The different widths of the vertical bars in (a) and (b) are for visual clarity, and have no significance. (c) Triangular distribution with 100 bins, a range of 1·00 mol m^{-2} s^{-1} (defined by g_{min} = 0·0 and g_{max} = 1·0), and a mode given by g_{peak} = 0·75. (d) Triangular distribution with 100 bins, a range of 0·40 mol m^{-2} s^{-1} (defined by g_{min} = 0·35 and g_{max} = 0·75), and a mode given by g_{peak} = 0·35. Note that (c) is an example of a 'left-skewed' distribution, and (d) is a 'right-skewed' distribution.

each distribution was varied by changing the minimum and maximum values of g. For example, the even distribution in Fig. 2a has a range of 1·0 mol m^{-2} s^{-1} (because g_{min} = 0·0 and g_{max} = 1·0), and the distribution in Fig. 2b has a range of 0·50 (g_{min} = 0·40 and g_{max} = 0·90).

Secondly, the *position* of a conductance distribution on the g axis was varied, also by changing the minimum and maximum g values. For example, the range (maximum g – minimum g) might be constant, say 0·50 mol m^{-2} s^{-1}, but that range could span the region from g = 0·0 to g = 0·50, or it might go from g = 0·40 to g = 0·90.

Finally, a feature that we termed *bimodality* was adjusted by dividing the patches into a variable number of groups, or 'bins'. For instance, a perfectly bimodal distribution would have two bins: half of the patches at the maximum value of conductance, and half at the minimum value (Fig. 2a). A more uniform (less bimodal) distribution would have a large number of bins (Fig. 2b). One additional set of model runs was performed wherein the patches were divided into two bins *unevenly*: the fraction of patches assigned to one bin (at g = 1·0) varied from zero to 100%, as the fraction assigned to the other bin (at various lower values of g) varied from 100% to zero (Fig. 3).

The second class of distributions examined were triangular distributions, which are similar to normal distributions in that a large number of patches lie near some peak conductance (called the 'mode') while progressively fewer patches have values of g that are farther away from this peak value. However, normal distributions have a curved relationship between frequency and conductance (often called 'bell-shaped'), and this relationship gradually tails off at large and small values of g. Triangular distributions have a more simple form: the frequency decreases linearly as g moves away from the peak value. Their relative frequency histograms thus appear triangular, as in Figs 2c and 2d.

Three features of triangular distributions were varied. As with even distributions, these variable features included the range and the *position* of this range on the g axis, and both were varied by changing the minimum and maximum values of conductance. The third feature that was varied for triangular distributions was 'skewness.'

Skewness is determined by the relative position of the peak frequency (mode) within the conductance range. For example, if the mode were equal to the minimum conductance, the distribution would look like a ramp sloping down to the right (as in Fig. 2d). Such a distribution would be called 'right-skewed.' If the mode were exactly halfway between the minimum and maximum values for g, the distribution would be non-skewed, and if the mode were closer to the high end of the g range, it would be left-skewed (as in Fig. 2c).

The manner in which all of these distributions, even and triangular, were adjusted numerically is described in Appendix C. For ease of reference, the information in Appendix C is summarized in Table 2.

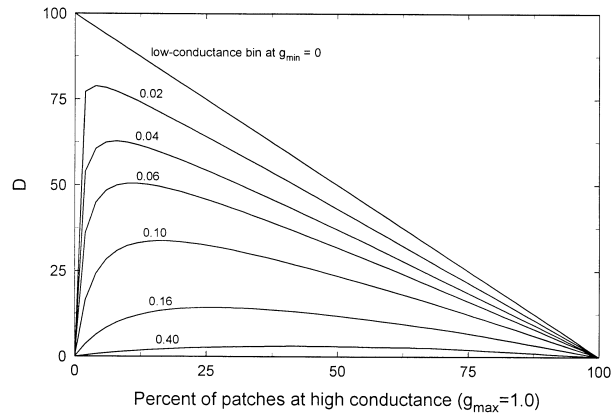

Figure 3. Plots of D (percentage difference between A_h and A_p) predicted for the model for perfectly bimodal distributions (two conductance bins). One thousand patches were assigned in varying proportions to the high-conductance and low-conductance bins. Each curve corresponds to a different value of g for the low-conductance bin, ranging from zero (the highest curve on the graph, a straight line) to 0·40. Plotted on the horizontal axis is the proportion of patches (expressed as a percentage of the total number of patches) that were assigned to the high-g bin (g = 1·0), ranging from 0% (all patches in the low-g bin) to 100% (all patches open at g = 1·0). Note that, although the line for g_{min} = 0 intersects the y axis, suggesting that D = 100% when the proportion of high-g patches is 0%, this is an artefact of the way in which the data have been presented; D should in fact equal zero at this point, as all of the patches are closed.

Figures	g_{min}	g_{max}	g_{peak}	Bins
4a	0	0·02 to 1·00	n/a	2–51
4b	0 to 0·98	1·00	n/a	2–51
4c	0 to 0·50	g_{min} + 0·50	n/a	2–51
6a	0	0·02 to 1·00	g_{min} to g_{max}	100
6b	0 to 0·98	1·00	g_{min} to g_{max}	100
6c	0 to 0·50	g_{min} + 0·50	g_{min} to g_{max}	100

Table 2. Variation of conductance distribution parameters used to generate surfaces of the difference between A_h and A_p (Figs 4 & 5)

RESULTS

Most conductance distributions caused fairly small differences (D) between A_h and A_p for a given c_i, with the parameter values for the assimilation model given in Appendix A. However, these differences often increased sharply as distribution parameters approached limiting values. Several qualitative trends were revealed between D and distribution features: D was generally larger for distributions that (1) spanned regions of lower conductance, (2) had larger ranges, (3) were more nearly bimodal (for even distributions), and (4) were right-skewed (for triangular distributions). Varying the parameters of the photosynthesis model (see Appendix A and Table 1) changed these relationships quantitatively, but not qualitatively. These general relationships are discussed in detail below.

Even distributions

The percentage difference (D) between A_h and A_p at a given c_i generally increased monotonically as the conductance distribution shifted down the g axis (spanning regions of lower conductance), as the distribution's range increased, and as distributions became more bimodal (Figs 4a–c). Where these trends conflicted with each other, and a shrinking range coincided with a shift down the g axis towards regions of lower conductance (as in Fig. 4a; see below), the latter effect dominated and D increased monotonically. For even distributions with the minimum conductance (g_{min}) held equal to zero (Fig. 4a), D increased monotonically as g_{max} was decreased from 1·00 to 0·02, and as the number of conductance bins (b) decreased from 51 to 2. The percentage difference was constant at its maximum value of 50% for all values of g_{max} when conductance was perfectly bimodal (b = 2) (Fig. 4a). For even distributions with g_{max} fixed at 1·0 mol m^{-2} s^{-1} (Fig. 4b), D increased monotonically with decreasing g_{min} and with decreasing b, to a maximum of 50% difference at 2 bins (a bimodal distribution) and g_{min} = zero. When a constant range ($g_{max} - g_{min}$) equal to 0·50 was shifted along the g axis (by varying g_{min} between zero and 0·50) (Fig. 4c), D again increased monotonically with decreasing g_{min} and with decreasing b.

Model runs with uneven bimodal distributions (two conductance bins, at g_{min} and g_{max}, containing different numbers of patches) showed that D can exceed 50%, and in fact can approach 100% for bimodal distributions (Fig. 3). Several curves relating D to the proportion of patches in the high-conductance bin (g_{max} = 1·0) are given in Fig. 3; each curve corresponds to a different value of g_{min} (the value of g for the low-conductance bin) ranging from zero to 0·40. D was largest for distributions that had a large number of patches at a low conductance, and a small number of patches at g_{max} = 1·0. When the low-conductance bin was set at g_{min} = 0, D increased linearly from zero to a limiting value of 100% as the proportion of patches in the high-g bin (g_{max} = 1·0) decreased from 100% to zero (note, however, that when this proportion is zero and all patches are thus closed, D is zero as well). For small non-zero values of g in the low-conductance bin, D increased in a curvilinear fashion with decreasing number of patches in the high-g bin, but D eventually declined sharply back to zero as the proportion of high-g patches approached zero. When the low-g bin was set at values larger than about g_{min} = 0·40, D was very small and nearly constant for any proportion of high-g versus low-g patches.

Triangular distributions

Larger differences were observed for triangular distributions that spanned regions of lower conductance, had broader ranges, and were right-skewed (Figs 5a–c). As distributions shifted from being left-skewed to being right-skewed for any given set of values for g_{min} and g_{max} (i.e. as g_{peak}, the mode of the distribution, was decreased from g_{max} to g_{min}), D increased monotonically (Figs 5a–c). Similarly, D increased as the range was adjusted to span regions of lower conductance (when g_{min} was held equal to zero and g_{max} was decreased from 0·02 to 1·00 for any given relative mode position; Fig. 5a). As was observed with even distributions, D increased as the distribution range became larger [as g_{min} decreased either for constant g_{max} = 1·00 (Fig. 5b) or for constant ranges (Fig. 5c)], as long as this change did not conflict with a shift towards lower conductance (as it did in Fig. 5a). D increased as fixed-range triangular distributions were shifted down the g axis (spanning regions with lower values of conductance) (Fig. 5c).

Different model parameter regimes

Qualitatively similar results were predicted by the model when different parameter sets were used. For example, setting the parameter J (see Table 1) to a low value made the biochemical assimilation model electron transport-limited

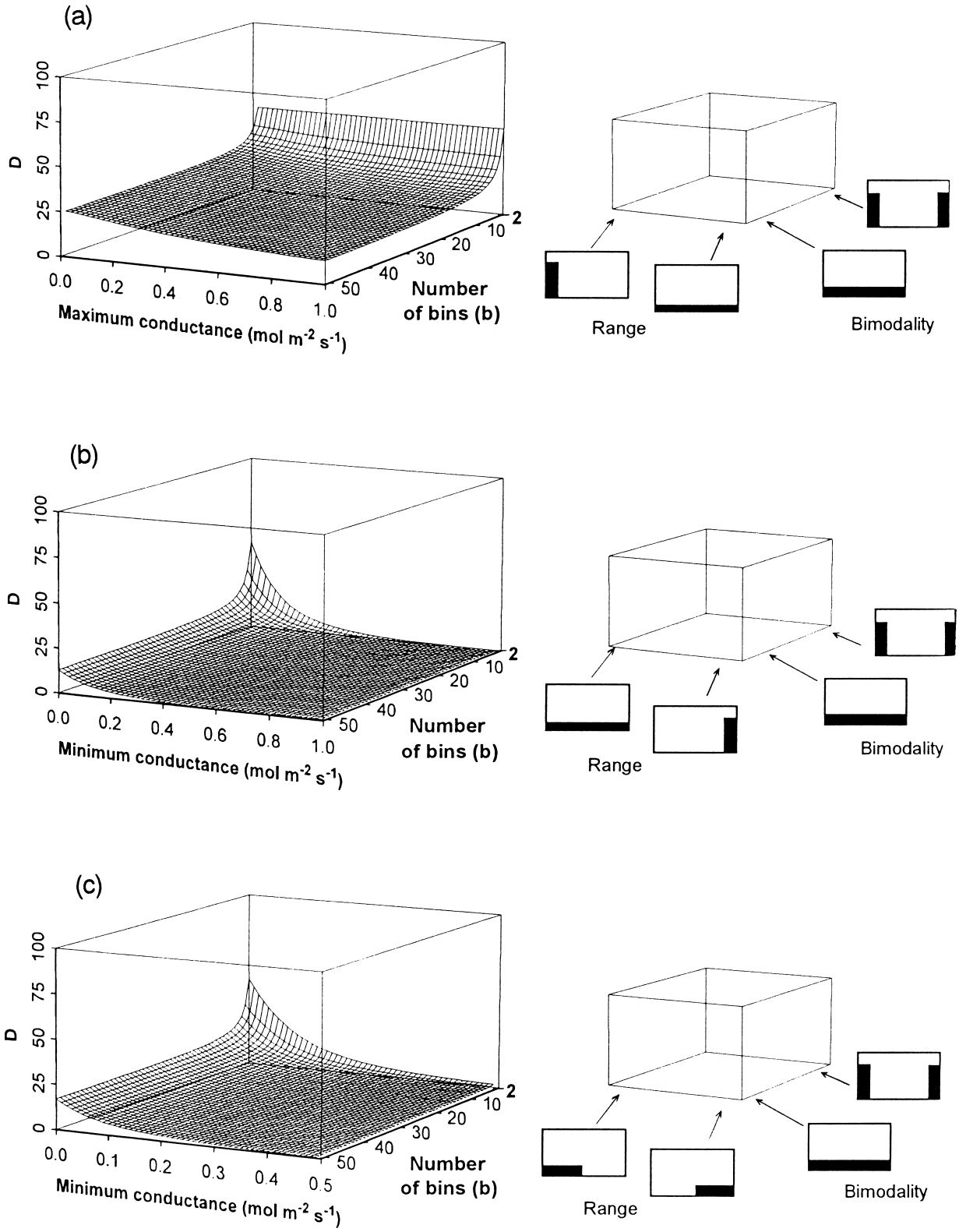

Figure 4. Surface plots of D (percentage difference between A_h and A_p, Eqn A9) predicted by the model for even conductance distributions, with the distribution range parameters g_{min} (minimum conductance in range) and g_{max} (maximum conductance) set or varied as follows: (a) fixed g_{min} (zero), variable g_{max} (ranging from 0·02 to 1·00); (b) variable g_{min} (ranging from zero to 0·98), fixed g_{max} (1·00); (c) constant-magnitude range ($g_{max} - g_{min} = 0{\cdot}50$); the position of this range was shifted by varying g_{min} from 0·00 to 0·50. In each case, the number of conductance bins was varied from 2 to 51. The diagrams to the right of each surface plot illustrate the qualitative differences between conductance distributions at the opposite ends of each axis.

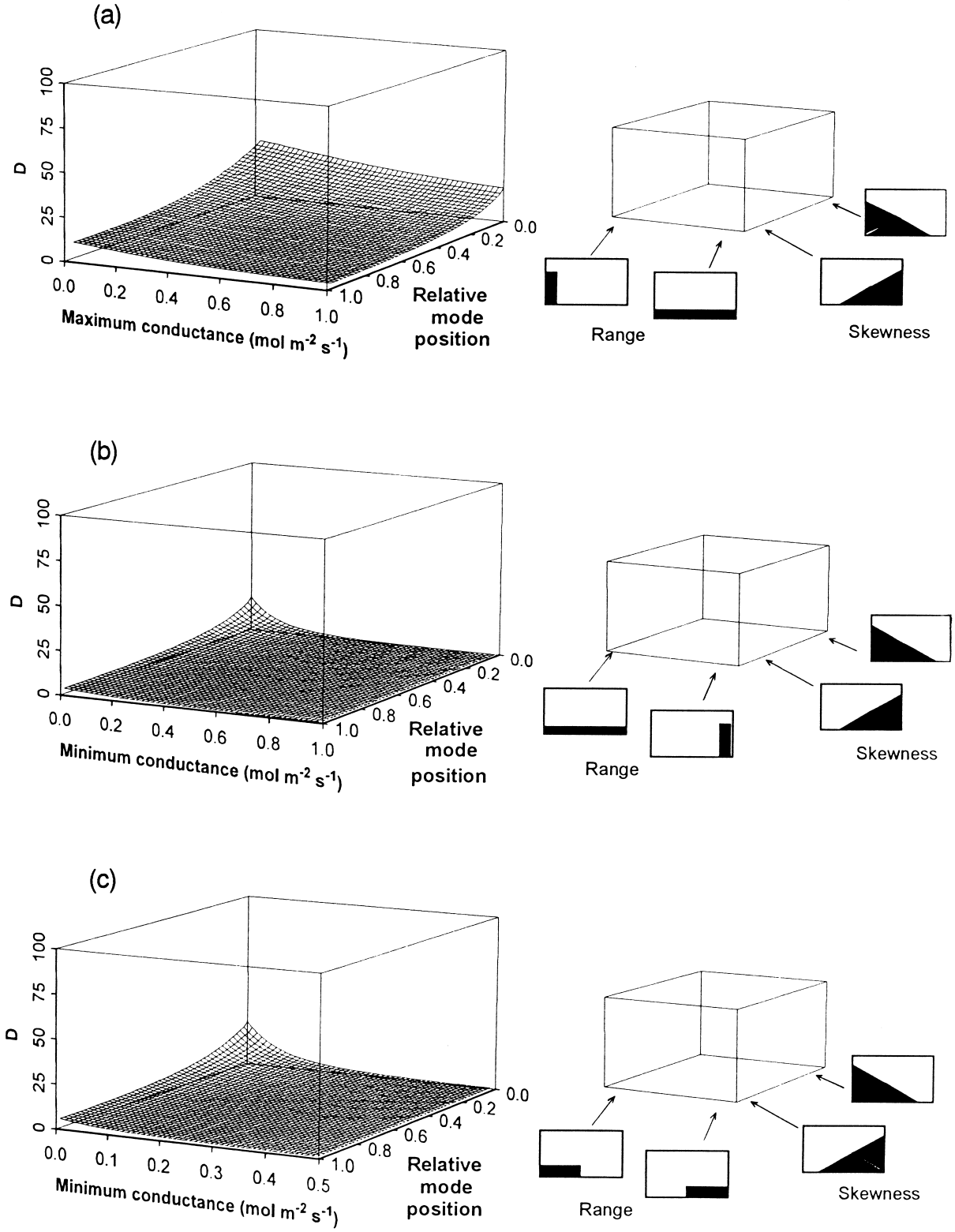

Figure 5. Surface plots of D (percentage difference between A_h and A_p) predicted by the explicit assimilation model using triangular conductance distributions with the distribution range parameters g_{min} (minimum conductance in range) and g_{max} (maximum conductance) set or varied as follows: (a) fixed g_{min} (zero), variable g_{max} (ranging from 0·02 to 1·00); (b) variable g_{min} (ranging from zero to 0·98), fixed g_{max} (1·00); (c) constant-magnitude range ($g_{max} - g_{min} = 0{\cdot}50$); the position of this range was shifted by varying g_{min} from 0·00 to 0·50. In each case, the mode (g_{peak}) was varied between g_{min} and g_{max} in 50 increments of equal size; the 'relative mode position' is given by the following expression: $(g_{peak} - g_{min})/(g_{max} - g_{min})$. One hundred conductance bins were used for all distributions. The diagrams to the right of each surface plot illustrate the qualitative differences between conductance distributions at the opposite ends of each axis, as in Fig. 4.

over most of the g range (Fig. 6). Despite this parameter change, the surfaces predicted by the model for low values of J (not shown) were essentially identical to those shown in Figs 3–5, which were generated from a purely Rubisco-limited model (J = 300 μmol e^- m^{-2} s^{-1}). The qualitative relationships between distribution features and D were therefore independent of the parameter sets used in the biochemical model.

Conductance distributions from real leaves

To help the reader understand the abstract mathematical analysis presented above, and to relate the analysis to real leaves, we used a computational method similar to the modelling procedure to predict differences between A_h and A_p for stomatal conductance distributions that were determined from chlorophyll fluorescence images of excised leaves of crabapple (*Malus dolgo* var. Spring Snow). Stomatal patchiness in these leaves was induced by the application of ABA through the petiole. This treatment resulted in a patchy distribution of chlorophyll fluorescence and a transient deviation from the A versus c_i curve determined before application of ABA (see Appendix B & Mott 1995 for details of this procedure). One fluorescence image for each of the two treatments described in the 'Materials and methods' section was chosen for detailed analysis. Each image corresponded to the largest departure of A and c_i data from the previously determined A versus c_i for that leaf. Figure 7 shows these two conductance distributions. Both are roughly triangular in form, but the first distribution (shaded in Fig. 7a; 14 May 1992) is slightly more right-skewed than the second distribution (shaded in Fig. 7b; 25 June 1992), and it is shifted towards the low end of the g axis (i.e. it is rooted at zero conductance).

In the first leaf (14 May, with conductance distribution shaded in Fig. 7a) the leaf photosynthetic rate (A_p) at the time that the image was taken was ≈40–70% of the value (A_h) predicted by a homogeneous $A(c_i)$ curve for the c_i inferred from gas-exchange calculations. In other words, gas-exchange measurements show that D equals roughly 30–60% for the distribution given in Fig. 7a. (These broad ranges resulted from variability in the estimation of c_i caused by the compounding of uncertainties in c_a, A and g). When the computational procedure described in Appendix B was used to predict differences between A_h and A_p for the same distribution, a range of 36–52% was predicted for D (Fig. 7a, inset). (In this case, the range for D is caused by scatter in the q_n image data, and is explained in detail in Appendix B). In the second leaf (with conductance distribution given in Fig. 7b) the range of values for D calculated by gas exchange extends from –3 to 8%, and the model predicts a value of 8% (Fig. 7b, inset).

This exercise illustrates the *qualitative* trend, described above and shown in Figs 3–5, between the distribution feature we have described as 'position' and the magnitude of D: the 14 May distribution is positioned closer to zero on the g axis, and is predicted to have a much larger value of D, as shown by gas-exchange measurements.

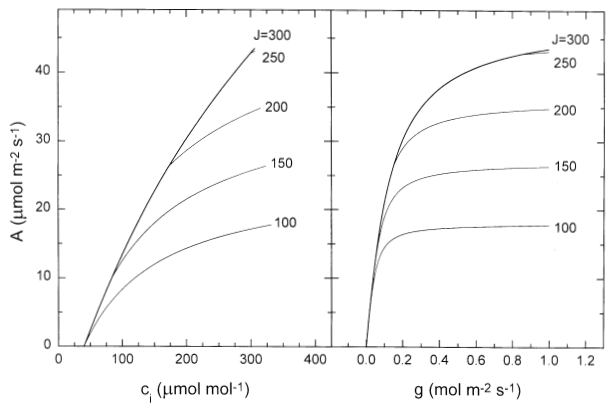

Figure 6. Several plots of the relationship between A and c_i, and between A and g, for the homogeneous model described in Appendix A. Each plot corresponds to a different value for J, with all other parameters given in Table 1. In all cases g was varied from zero to 1·0 mol m^{-2} s^{-1}. The $A(c_i)$ and $A(g)$ curves given here show that the transition from Rubisco limitation to electron-transport limitation does not occur for g (1·0 mol m^{-2} s^{-1} when J = 300; the modelling results presented in this study were obtained using a value of J = 300, so the curves for J = 300 are plotted with thicker lines.

DISCUSSION

Terashima *et al.* (1988) showed that the curved relationship between A and g is ultimately responsible for 'spurious depressions' in the $A(c_i)$ curve caused by stomatal patchiness. Using the example of a leaf with two groups of patches, each at a different conductance, they showed that the mean assimilation rate for such a leaf would not fall on the $A(g)$ curve associated with a homogeneous leaf, but would instead be lower. Farquhar (1989) formalized this problem and extended it to the general case. He showed that the value of c_i measured by gas exchange is a 'conductance-weighted' spatial average, whereas an average c_i weighted by carboxylation efficiency (i.e. photosynthetic capacity) would be more useful for relating changes in A to changes in mesophyll capacity (Farquhar 1989). Despite these arguments, which explained and thereby validated data showing declines in the $A(c_i)$ curve during patchy stomatal closure, Cheeseman (1991) concluded that heterogeneous stomatal closure can only cause small depressions in the $A(c_i)$ curve. More recently, Mott (1995) showed that both calculated and measured assimilation rates could be reduced by as much as 50% by patchy stomatal conductance in some leaves, but not in others. [These results were obtained at low partial pressures of O_2, which can change the appearance of the $A(c_i)$ curve. However, running our model at low O_2 did not cause significantly larger differences to be observed between A_h and A_p (data not shown), so the large deviations from the $A(c_i)$ curve observed by Mott (1995) were probably not caused by this factor but rather by some feature of the conductance distri-

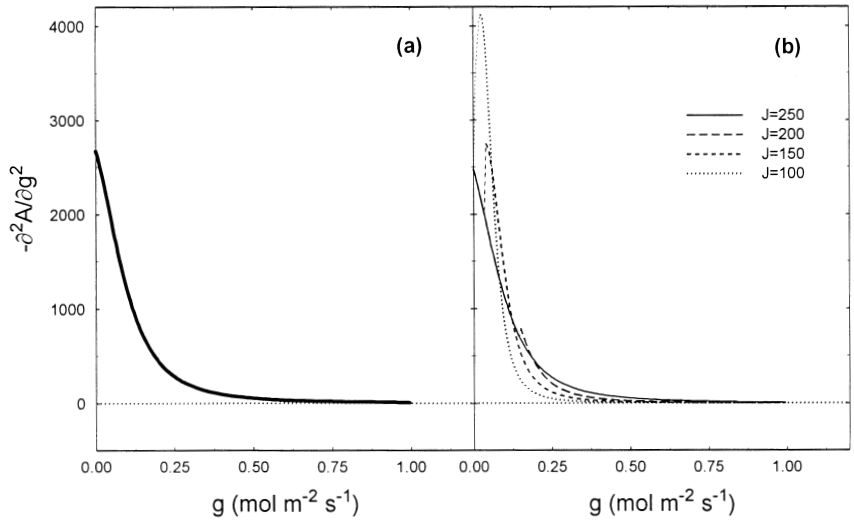

Figure 7. The curvature of the function $A(g)$ (presented here as the absolute magnitude of the second derivative of A with respect to g) given by the model of photosynthesis described in Appendix A. For $J \geq 250$, the curvature is largest at $g = 0$ and monotonically approaches zero with increasing g. (a) $J = 300$; (b) $J = 100$, 150, 200, 250. The only qualitative difference between the curves for high values of J and those for low values is a slight jump discontinuity in the low-J curves at the conductance where the transition between electron transport limitation and Rubisco limitation occurs. Modelling results (not shown) verified that this discontinuity did not affect the monotonic dependence of D on distribution features shown in Figs 4–6. [Units for the derivative are μmol m^{-2} s^{-1} (mol m^{-2} s^{-1})$^{-2}$].

butions.] The analysis presented here reconciles these apparently contradictory conclusions by extending Cheeseman's analysis to non-normal conductance distributions.

Our data relating the difference between A_h and A_p at a given c_i to various distribution features are consistent with the suggestion of Terashima *et al.* (1988) that the curvature of the $A(g)$ relationship is responsible for causing depressions in the $A(c_i)$ curve. This can be explained by considering the second partial derivative of A with respect to g, which is a measure of the curvature of $A(g)$. Larger differences were predicted for distributions that spanned regions of lower conductance, and Fig. 8 shows that the $A(g)$ relationship is most highly curved at low values of conductance. These results are also consistent with data showing that depressions in the $A(c_i)$ curve are more common under stressed conditions, which tend to promote low stomatal conductance (e.g. Raschke *et al.* 1990; Beyschlag *et al.* 1992; Pospisilova & Santrucek 1994; Cardon *et al.* 1994).

The model also revealed that the *skewness* of a conductance distribution influences the $A(c_i)$ relationship measured by gas exchange. Specifically, right-skewed distributions (those for which the mode is closer to the lower end of the range, as in Fig. 2d) produce greater deviations than left-skewed distributions. This is also consistent with the contention that the curvature of $A(g)$ is important in causing changes in the observed relationship between A and c_i: larger curvature is observed at low values of conductance (Fig. 8), so the large number of patches at low conductances in right-skewed distributions should cause a greater difference between A_h and A_p at a given c_i.

Another important distribution feature revealed in the preceding analysis was a property that we termed 'bimodality.' Distributions with a small number of conductance bins, or modes, tend to produce larger differences between A_h and A_p, with the extreme case being perfect bimodality (two distinct groups of conductance patches). Differences of up to 50% were calculated for even bimodal distributions; these values approached 100% for uneven bimodal distributions with a large number of nearly closed stomata and only a few open stomata. Again, these results agree with the observation that deviations from the $A(c_i)$ curve are more likely to occur under stressed conditions, which are associated with lower conductance.

Conductance distributions from real leaves

When conductance distributions obtained from chlorophyll fluorescence images of real leaves were used in the model, the predicted values or ranges of D were similar to those calculated from gas-exchange data (Figs 7a & b, inset). These results provide a real system to which we can apply the relationships described above between distribution features and changes in the relationship between A and c_i. In the data from 14 May 1992 (Fig. 7a), relatively large values of D were predicted (36–52%) and observed (30–60%). In contrast, fairly small values were predicted (8%) and observed (–3 to 8%) for the data from 25 June 1992 (Fig. 7b). We can now ask the question: are there recognizable features of these conductance distributions that can help explain these differing values of D?

The 14 May distribution is shown in Fig. 7a. It can be described as a roughly triangular distribution rooted at

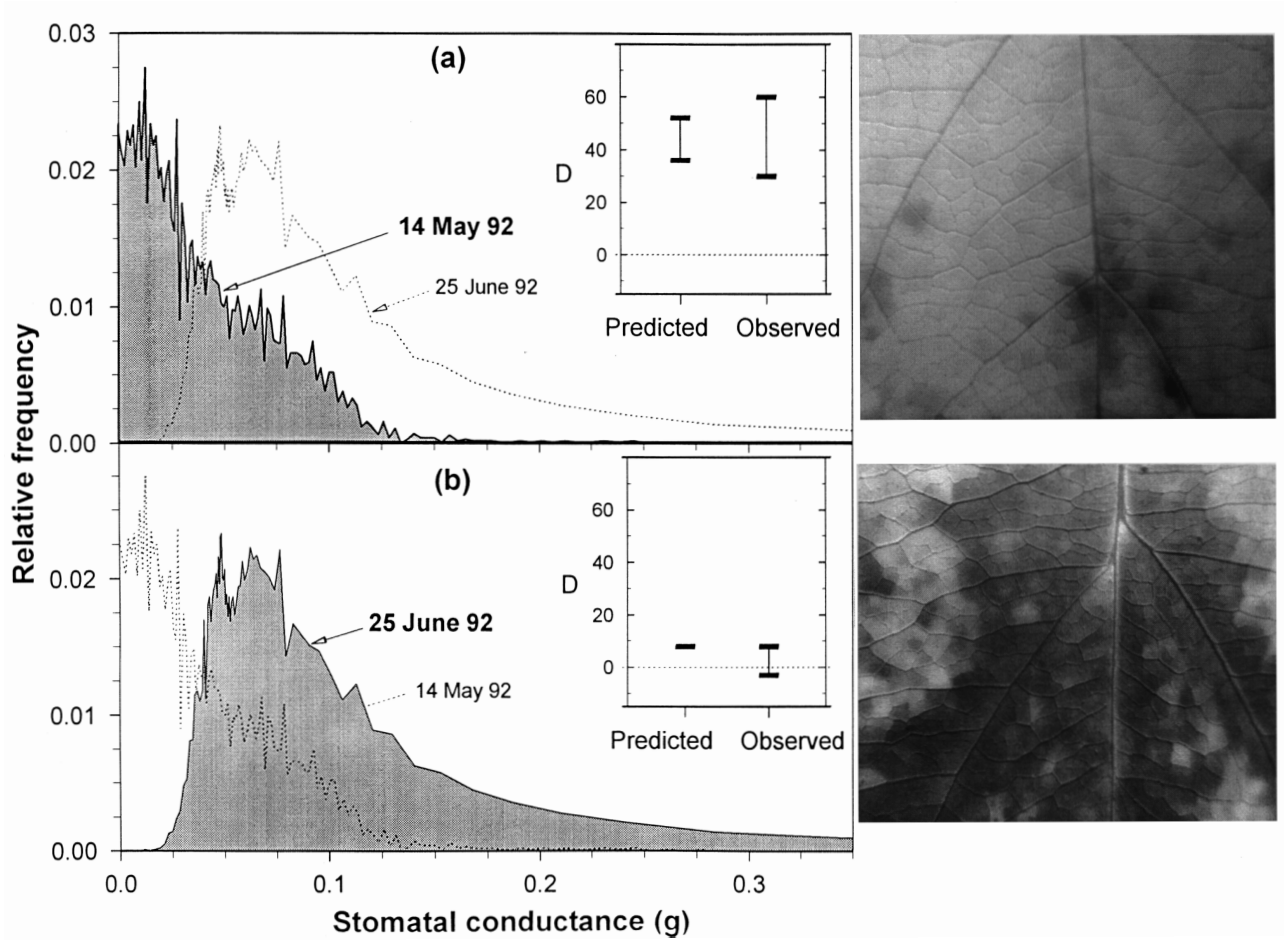

Figure 8. Relative frequency distributions for stomatal conductance, calculated from images of chlorophyll fluorescence obtained from excised leaves of crabapple (*Malus dolgo* var. Spring Snow) after applying a pulse of 10 mmol m^{-3}ABA [45 s, total dose = 20 nmol m^{-2} (14 May); 62 s, total dose = 15 nmol m^{-2} (25 June)] to the transpiration stream. (a) Conductance distributions from 14 May 1992 (solid line and shading) and from 25 June 1992 (dotted line). Both distributions are shown in (a) and (b) so that they may be directly compared. (a, inset) Ranges of *D* predicted by the model for the 14 May distribution (at left) and observed by gas exchange (at right). (b) Conductance distributions from 25 June 1992 (solid line and shading) and from 14 May 1992 (dotted line). (b, inset) Ranges of *D* predicted by the model for the 25 June distribution and observed by gas exchange. The q_n images for 14 May and 25 June are shown to the right of (a) and (b), respectively.

g_{min} = 0, with a mode (g_{peak}) very nearly at zero conductance. As described previously, modelling results showed that differences between A_h and A_p were greatest for triangular distributions that spanned regions of low conductance, were right-skewed, and had broad ranges. Clearly, the distribution in Fig. 7a spans regions of low conductance and is right-skewed. In contrast, the distribution from 25 June 1992 (Fig. 7b), which yielded much smaller values of *D*, is located farther to the right on the *g* axis, and also appears slightly less right-skewed (because it does not terminate abruptly at zero conductance). These fairly small but distinct differences in the character of the two distributions were apparently sufficient to cause large differences in the observed relationships between A_h and A_p.

While this analysis suggests that distributions causing large deviations (30–60%, Fig. 7a) actually occur in real leaves, it would be premature to conclude this from such a brief analysis. Rather, we merely suggest that such questions could be effectively addressed with this sort of analysis.

General applicability of the model

The curvature of $A(g)$ emerged in the preceding discussion as a major variable controlling differences between A_h and A_p. Although the $A(g)$ map is defined in part by the biochemical model, we found that different parameter regimes for this model did not generally change the qualitative nature of the curvature (Fig. 8b shows the curvature for four different values of *J*, ranging from 100 to 250 μmol e^- m^{-2} s^{-1}). Thus, the qualitative aspects of the results presented here should be applicable to a wide range of C_3 leaves. However, two factors (heterobaric versus homobaric leaves, and patch size) may influence the quantitative aspects of these results. Our model assumes the leaf to be perfectly heterobaric. That is, patches are separated by bundle sheath extensions, which block diffusion of CO_2

among patches. For leaves without bundle sheath extensions (homobaric) or for those with incomplete bundle sheath extensions, the effects of patchy stomatal closure on gas exchange will be reduced. However, diffusion of CO_2 among patches may be slow enough to ignore for many large patches (> 100 μm across), particularly in leaves with densely packed mesophyll (Parkhurst 1994). The exact deviation from the perfectly heterobaric leaf will therefore depend on both the patch size and the internal anatomy of the leaf.

Summary

The results presented here have identified several *qualitative* features of stomatal conductance distributions that are important in determining the difference in assimilation rate between a leaf with patchy stomatal conductance (A_p) and a leaf with homogeneous stomatal conductance (A_h) at the same value of c_i. The relevant trends concerning these distribution characteristics can be summarized as follows. Differences between A_h and A_p tend to be greater for conductance distributions that (1) span regions of lower conductance, (2) extend over a larger range of conductance (except when decreasing the range also causes a distribution to span regions of lower conductance, i.e. when g_{max} is decreased while g_{min} is held constant), (3) are more nearly bimodal, and (4) are right-skewed. These differences can be arbitrarily large, approaching 100% for uneven bimodal distributions with many patches at a very low conductance and only a few patches at high conductance.

In agreement with the results presented by Cheeseman (1991), this study concludes that many heterogeneous or 'patchy' conductance distributions do not produce large differences between A_h and A_p. This introduces yet another element of uncertainty into the interpretation of gas-exchange data. Whereas deviations from the 'homogeneous' $A(c_i)$ curve have been shown to be ambiguous indicators of changes in a leaf's mesophyll capacity, the results described here show that the *absence* of such deviations is an ambiguous indicator of homogeneous stomatal behaviour.

Perhaps more importantly, this study provides an explanation for the apparent contradiction between Cheeseman's (1991) conclusion that stomatal heterogeneity has little effect on gas-exchange calculations, and data showing large effects (e.g. Terashima *et al.* 1988; Raschke *et al.* 1990; Beyschlag *et al.* 1992; Epron & Dreyer 1993; Mott 1995). It is now clear that some kinds of stomatal conductance distributions can cause large changes in the relationship observed between A and c_i by gas-exchange calculations, and the available evidence suggests that such distributions may exist. This result does not imply that all changes in the A *versus* c_i relationship are caused by stomatal patchiness; such changes may of course also result from changes in mesophyll functioning. However, it does show that one cannot rule out patchy stomatal closure as the cause for large changes in the A *versus* c_i relationship, particularly when measured stomatal conductance changes concurrently. Future efforts should focus on testing rigorously any apparent coincidence of patchiness and changes in the $A(c_i)$ curve. This may be accomplished in part by comparing changes observed by gas exchange with changes predicted by a model for the observed conductance distributions.

APPENDIX A: ASSIMILATION MODELLING PROCEDURE

The modelling procedure used to calculate the difference between A_h and A_p at a single value of c_i was similar to that employed by Cheeseman (1991). This procedure is described heuristically in the 'Materials and methods' section; here we present the mathematical details in a somewhat more rigorous form. For a given model run (corresponding to a single moment in time, for one leaf) a discrete distribution of conductances was generated for an array of 950–1000 'patches' (this number varied between 950 and 1000 because a 'remainder' often exists, and is discarded, when 1000 patches are divided into groups of equal size containing whole numbers of patches). Each element k in this array represented a patch of equal leaf area with a single set of values for conductance (g_k), intercellular CO_2 mole fraction (c_{ik}) and assimilation rate (A_k). The conductance for each patch was specified by a chosen conductance distribution, and c_{ik} and A_k were calculated from g_k. using a coupled biochemical/diffusion model.

The biochemical assimilation model of Farquhar, von Caemmerer & Berry (1980) (eqns A1 and A2) was used to model the relationship between A and c_i for homogeneous regions of the leaf (i.e. individual patches, or in the non-patchy case, the entire leaf). Equation A1 represents the Rubisco-limited phase of the biochemical model, and Eqn A2 represents the electron transport-limited phase:

$$A_v = \frac{V_{c,max}\,(c_i - \Gamma_*)}{c_i + K_c\,(1 + O/K_o)} - R_d, \qquad \text{(A1)}$$

$$A_J = \frac{J\,(c_i - \Gamma_*)}{4\,(c_i + 2\Gamma_*)} - R_d. \qquad \text{(A2)}$$

A simplified 'supply' function (A_S) was used to model CO_2 diffusion into leaves:

$$A_s = g\,(c_a - c_i), \qquad \text{(A3)}$$

where c_a is the ambient CO_2 partial pressure. In Eqn A3 and throughout this paper, g refers to the stomatal conductance to CO_2 diffusion. Boundary layer resistance was assumed to be negligibly small. The variables and parameters in Eqns A1 to A3 are described in Table 1, and their numerical values are given in Table 1 where appropriate. The biochemical and diffusion models were solved simultaneously by extracting the variable c_i from each equation, combining the resulting equations, and solving for A with the quadratic formula. By linking the two models in terms of a single common parameter (g) that identifies the point where they intersect, this yielded 'intersection functions' ['$(A_V \cap A_S)$' and '$(A_J \cap A_S)$'] giving A as a function of g

(two functions were generated because the procedure was repeated for both Eqns A1 and A2). The assimilation rate corresponding to a given value of g was taken as the minimum of these two intersection functions (Eqn A4):

$$A_k = A\,(g_k) = \min\{(A_v \cap A_s)\,(g_k), (A_j \cap A_s)\,(g_k)\}. \quad \text{(A4)}$$

The second, third and fourth partial derivatives of A with respect to g were obtained analytically from the $A(g)$ relationship given by Eqn A4. Several plots of $A(g)$ and the associated plots of $A(c_i)$ are given in Fig. 6; each pair corresponds to a different value for J (see Table 1).

Equation A4 was used to calculate the assimilation rate $A_k = A(g_k)$ for each patch k. These A_k were then averaged over the leaf surface to give A_p, the value of A that would be calculated by standard gas-exchange techniques (Eqn A5):

$$A_p = \frac{\sum_{k=1}^{n} A(g_k)}{n}, \quad \text{(A5)}$$

where n is the total number of patches. The intercellular CO_2 partial pressure that would be measured by gas-exchange techniques for the patchy leaf (c_{ip}) was obtained by solving the CO_2 diffusion equation for c_i, using the whole-leaf values for assimilation and conductance:

$$c_{ip} = c_a - \frac{A_p}{g_{average}} \quad \text{(A6)}$$

The whole-leaf conductance value ($g_{average}$ in Eqn A6) was calculated as the arithmetic mean of all individual patch conductances:

$$g_{average} = \frac{\sum_{k=1}^{n} g_k}{n}, \quad \text{(A7)}$$

The assimilation rate that would be observed under conditions of homogeneous stomatal conductance in association with c_{ip} (A_h) was calculated directly from the biochemical model as the minimum of the two CO_2 'demand' functions A_V and A_J evaluated at c_{ip}:

$$A_h = \min\{A_v(c_{ip}), A_J(c_{ip})\} \quad \text{(A8)}$$

Finally, the percentage difference (D) between A_h and A_p was calculated from Eqn A9:

$$D \equiv \%\ Difference = 100 \times \frac{(A_h - A_p)}{A_h} \quad \text{(A9)}$$

APPENDIX B: PROCEDURES FOR ANALYSING DATA FROM REAL LEAVES

Images of chlorophyll fluorescence were obtained from excised leaves of *Malus dolgo* (var. Spring Snow) and converted to 'q_n' images as described in Mott (1995). Empirical relationships were determined for non-patchy leaves between q_n and c_i, and between A and c_i. The q_n versus c_i data were fitted to polynomial functions, and the A versus c_i data were fitted to modified Michaelis-Menten functions. For each patchy leaf, several qN images were obtained over a period of time following the application of a pulse of ABA to the transpiration stream, during which gas-exchange measurements were changing rapidly; the image taken closest to the instant of maximum observed deviation from the non-patchy A versus c_i curve was chosen for detailed analysis. Relative frequency histograms for q_n were calculated from these q_n images. The pixel intensity (q_n) in these images could take any integer value from 0 to 255, so there were effectively 256 'q_n bins'. For each of these bins, the q_n versus c_i polynomials were used to calculate a value of c_i, the A versus c_i equations were used to calculate a value of A, and finally the simple diffusion equation (Eqn A3) was used with the appropriate value of c. (290 μmol mol^{-1} for 14 May 1992, and 320 μmol mol^{-1} for 25 June 1992) to solve for a value of g. Note that this procedure for calculating g involves the use of two empirical equations (qN versus c_i, and A versus c_i), each of which has some degree of sampling error associated with it. We did not attempt to quantify this error because (1) no quantitative conclusions are being drawn from these data, and (2) quantifying the error would make it impossible to express the resulting g distributions in a clear and simple manner, negating the purpose of this exercise (to clarify the mathematical modelling analysis presented in the text, and relate it to real leaves).

The conductance distributions thus generated were used in the model to predict values of A_h and A_p, as follows. The value of A for each bin was multiplied by the relative frequency corresponding to that bin (the fraction of the total number of pixels with the associated value of q_n), and these values were summed to give A_p, the total leaf assimilation rate. The value of c_i that would be measured by gas exchange (and that would normally be used to predict an assimilation rate from the non-patchy A versus c_i curve) equals the conductance-weighted c_i (Eqn A7; Farquhar 1989); this value was calculated directly by summing the products of c_i, g and the relative frequency for each bin, and dividing this sum by the sum of the products of g and the relative frequency for each bin. This conductance-weighted c_i was then applied to the empirically determined non-patchy A versus c_i curve for the leaf, and the percentage difference between the resulting predicted values for A_h and A_p was calculated as in Eqn A10 to give D. This was compared with the value of D observed by gas exchange.

Because of scatter in the q_n image data from 14 May 1992, a large number of pixels were observed that corresponded to a value of zero for conductance, whereas in theory only one value of q_n should be observed for each c_i and thus for each g value. Furthermore, because some of these pixels probably correspond to regions of the leaf with non-zero conductance and/or to veins (which appear bright due to an artefact but which do not support photosynthesis), their inclusion in the $g = 0$ bin gives disproportionately large weight to this bin; this causes the relative frequency histogram in Fig. 7a to have a very large and artefactual 'spike' at $g = 0$. This in turn will lead to an overestimation of D, because regions of the leaf with closed stomata lower

the value of A measured by gas exchange while not affecting the value of c_i. To account for this, we calculated two values of D for the 14 May distribution: one with this spike at $g = 0$, and one without the spike but with the value for frequency corresponding to the adjacent q_n bin. Since the pixels that were omitted in the second case probably represented values of g near zero, we believe that the value of D calculated without the $g = 0$ spike represents a minimum difference between A_h and A_p; conversely, the value of D from the distribution *with* the spike at $g = 0$ corresponds to a maximum difference. It was not necessary to calculate two values of D for the 25 June 1992 leaf, because the distribution did not run into the g axis, and it was assumed that any scatter in the q_n distribution had roughly neutral effects on the estimation of D.

APPENDIX C: HOW DISTRIBUTION FEATURES WERE ADJUSTED QUANTITATIVELY

The ranges and shapes of both even and triangular distributions were varied in three different ways. First, the range was varied by holding the minimum conductance (g_{min}) constant at zero and varying the maximum conductance (g_{max}) from 0·02 to 1·00 in 50 sequential model runs. Secondly, the range was varied by holding g_{max} constant at 1·0 mol m^{-2} s^{-1} and varying g_{min} from zero to 0·98. Finally, the position of a fixed range was varied by holding the range ($g_{max} - g_{min}$) constant at 0·50 mol m^{-2} s^{-1}, and allowing g_{min} to vary from 0·0 to 0·50.

Each of these series of 50 model runs was performed 50 different times, over a range of numbers of conductance bins (for even distributions) or relative positions of the mode (for triangular distributions). Each of the surfaces in Figs 4 and 5 therefore represents 2500 distinct model runs, and each of the curves in Fig. 3 represents 50 model runs. The manner in which conductance distributions were varied to generate the surfaces in Figs 4 and 5 is summarized in Table 2. Following is an explanation of how the number of conductance bins and the relative mode position were varied, and how this determined the exact conductance distribution used in each model run.

For even distributions, 1000 patches were divided evenly into a specific number of groups, or *conductance bins*. Each bin contained an equal number of patches, and all of the patches within any given bin shared a common value of conductance. To adjust the feature that we have termed 'bimodality,' the number of bins (b) was varied from 2 to 51, and these bins were distributed uniformly across the range. For example, if $b = 3$, $g_{min} = 0$ and $g_{max} = 1·0$, then 333 patches would have a conductance of $g = 0$, 333 would have $g = 0·50$, and 333 would have $g = 1·0$. This is equivalent to the following: $\upsilon(0·0) = \upsilon(0·5) = \upsilon(1·0) = 333$, where $\upsilon(g_b)$ denotes the frequency, or number of patches, assigned to a bin with conductance = g_b. The remainder of 1000/b (patches/bins) was discarded so that all bins had an equal, integer frequency. Two examples of discrete even distributions are shown in Figs 2a and 2b. The first of these (Fig. 2a) has two bins, and is therefore 'perfectly bimodal'; the second (Fig. 2b) is more uniform, with 14 bins.

To determine the effect of uneven bimodal distributions on the relationship between A and c_i, one additional set of curves was generated using distributions that had two bins, with the high-conductance bin constant at $g_{max} = 1·0$. Two features were adjusted between model runs for these bimodal distributions: the proportion of patches that were assigned to each of the two bins was varied between zero and 100%, and the low-conductance bin (g_{min}) was varied between zero and 0·98.

For triangular distributions, the total number of bins was always equal to 100, but the relative position of the mode (g_{peak}) was adjusted. This is best explained graphically (see Figs 2c & d), but to understand the visual examples given in Figs 2c and 2d we must first introduce the triangular frequency distribution function, as follows. The number of patches assigned to each of 100 conductance bins increased linearly from zero to 20 as conductance increased from g_{min} to g_{peak} (the mode), and decreased linearly from 20 back to zero as conductance increased from g_{peak} to g_{max}:

$$\nu(g_b) \leq \begin{cases} 20(g_b - g_{min})/(g_{peak} - g_{min}) & g_b \leq g_{peak} \\ 20(g_{max} - g_b)/(g_{max} - g_{peak}) & g_b > g_{peak} \end{cases} \quad \text{(C1)}$$

where the subscript b refers to a particular conductance bin. The '$\leq$' sign on the far left in Eqn C1 accounts for the fact that the frequency given by the right-hand side of Eqn C1 was rounded down to the nearest whole number. [The number 20 for the maximum frequency, $\upsilon(g_{peak})$, arises as a constant when integrating Eqn C1 and setting it equal to 1000 patches.] The feature called 'skewness' was varied simply by adjusting the mode (g_{peak}) between g_{min} and g_{max} in 50 equal steps. Figures 2c and 2d show two examples of the triangular distributions described here. Figure 2c is a 'left-skewed' distribution, and Fig. 2d is 'right-skewed'.

ACKNOWLEDGMENTS

We thank Jiri Santrucek for insightful comments on the subject, and Rand Hooper for excellent technical assistance.

REFERENCES

Beyschlag W., Pfanz H. & Ryel R.J. (1992) Stomatal patchiness in Mediterranean evergreen sclerophylls. Phenomenology and consequences for the interpretation of the midday depression in photosynthesis and transpiration. *Planta* **187**, 546–553.

Cardon Z.G., Mott K.A. & Berry J.A. (1994) Dynamics of patchy stomatal movements, and their contribution to steady-state and oscillating stomatal conductance calculated with gas-exchange techniques. *Plant, Cell and Environment* **17**, 995–1008.

Cheeseman J.M. (1991) PATCHY: simulating and visualizing the effects of stomatal patchiness on photosynthetic CO_2 exchange studies. *Plant, Cell and Environment* **14**, 593–599.

Daley P.F., Raschke K., Ball J.T. & Berry J.A. (1989) Topography of photosynthetic activity of leaves obtained from video images of chlorophyll fluorescence. *Plant Physiology* **90**, 1233–1238.

Epron D. & Dreyer E. (1993) Photosynthesis of oak leaves under water stress: maintenance of high photochemical efficiency of photosystem II and occurrence of non-uniform CO_2 assimilation. *Tree Physiology* **13**, 107–117.

Farquhar G.D. (1989) Models of integrated photosynthesis of cells and leaves. *Philosophical Transactions of the Royal Society of London B* **323**, 357–367.

Farquhar G.D., von Caemmerer S. & Berry J.A. (1980) A biochemical model of photosynthetic CO_2 assimilation in leaves of C_3 species. *Planta* **149**, 78–90.

Gunasekera D. & Berkowitz G.A. (1992) Heterogeneous stomatal closure in response to leaf water deficits is not a universal phenomenon. *Plant Physiology* **98**, 660–665.

Hirasawa T., Wakabayashi K., Touya S. & Ishihara K. (1995) Stomata responses to water deficits and abscisic acid in leaves of sunflower plants (*Helianthus annuus* L.) grown under different conditions. *Plant Cell Physiology* **36**, 955–964.

Mott K.A. (1995) Effects of patchy stomatal closure on gas exchange measurements following abscisic acid treatment. *Plant, Cell and Environment* **18**, 1291–1300.

Mott K.A., Cardon Z.G. & Berry J.A. (1993) Asymmetric patchy stomatal closure for the two surfaces of *Xanthium strumarium* L. leaves at low humidity. *Plant, Cell and Environment* **16**, 25–34.

Nobel P.S. (1974) *Introduction to Biophysical Plant Physiology*, pp. 308–309. Freeman, San Fransisco.

Parkhurst D.F. (1994) Tansley Review no. 65. Diffusion of CO2 and other gases inside leaves. *New Phytologist* **126**, 449–479.

Pospisilova J. & Santrucek J. (1994) Stomatal patchiness. *Biologia Plantarum* **36**, 481–510.

Raschke K., Patzke J., Daley P.F. & Berry J.A. (1990) Spatial and temporal heterogeneities of photosynthesis detected through analysis of chlorophyll-fluorescence images of leaves. In *Current Research in Photosynthesis*, Vol. IV (ed. M. Baltscheffsky), pp. 573–578. Kluwer Academic Publishers, the Netherlands.

Robinson S.P., Grant W.J.R. & Loveys B.R. (1988) Stomatal limitation of photosynthesis in abscisic acid-treated and in water-stressed leaves measured at elevated CO_2. *Australian Journal of Plant Physiology* **15**, 495–503.

Terashima I. (1992) Anatomy of non-uniform leaf photosynthesis. *Photosynthesis Research* **31**, 195–212.

Terashima I., Wong S.-C., Osmond C.B. & Farquhar G.D. (1988) Characterisation of non-uniform photosynthesis induced by abscisic acid in leaves having different mesophyll anatomies. *Plant Cell Physiology* **29**, 385–394.

van Gardingen P.R., Jeffree C.E. & Grace J. (1989) Variation in stomatal aperture in leaves of *Avena fatua* L. observed by low-temperature scanning electron microscopy. *Plant, Cell and Environment* **12**, 887–898.

van Kraalingen D.W.G. (1990) Implications of non-uniform stomatal closure on gas exchange calculations. *Plant, Cell and Environment* **13**, 1001–1004.

Woodrow I.E. & Berry J.A. (1988) Enzymatic regulation of photosynthetic CO_2 fixation in C_3 plants. *Annual Review of Plant Physiology and Plant Molecular Biology* **39**, 533–94.

Received 8 October 1996; received in revised form 7 January 1997; accepted for publication 21 January 1997